Appendix 3

DENSITY STRUCTURES IN "LOW INFLOW ESTUARIES"

John L. Largier
Scripps Institution of Oceanography
University of California

Cliff J. Hearn
Australian Defence Force Academy
University College of New South Wales

D. Bart Chadwick
Scripps Institution of Oceanography
University of California

ABSTRACT

The study of estuarine hydrodynamics has been dominated by a focus on the defining feature of estuaries - freshwater inflow. Low-inflow "estuaries" (LIE's), or semi-enclosed bays, have received very little attention in spite of their common occurrence. In this paper, we discuss the occurrence of LIE's as a seasonal feature in mediterranean-climate regions (e.g., California, USA).

Buoyancy fluxes are dominated by air-water exchange. There is competition between a positive buoyancy flux due to heating and a negative buoyancy flux due to evaporation. In spite of large thermohaline signals, the resultant buoyancy flux is often too weak to bring about vertical stratification and buoyancy-driven exchange in shallow estuarine basins. This results in very long residence times being observed in tidally sheltered waters, such as at the landward end of these LIE basins.

Through a simple model of surface fluxes and longitudinal dispersion in LIE's, we explain observed temperature, salinity and density structures in Tomales, San Diego, and Mission bays (California, USA) . In summary, we identify four regions: a marine region in the outer bay (dominated by tidal exchange with the ocean), a thermal region (where heating dominates the buoyancy flux), a hypersaline region (where evaporation dominates the buoyancy flux), and an estuarine regime (where freshwater inflow dominates the buoyancy flux). The clear

spatial separation of thermal and hypersaline regimes is owing to the different temporal structure of heating and evaporation in mediterranean-climate estuaries.

INTRODUCTION

In much the same way that people who study rivers in arid or semi-arid areas refer to them as water courses, recognizing that run-off is not persistent, so we too need to find a new term or re-define the old one (e.g., Pritchard, 1967) to allow for the fact that many "estuaries" do not experience a persistent freshwater inflow. In arid areas, or during the dry season in mediterranean climate regions, river inflow is negligible or absent. Any estuary-ocean density differences are due to differential heating or evaporation, i.e., due to surface buoyancy fluxes. With the anthropogenic extraction of water from rivers, more estuaries are becoming net evaporative (i.e., the fresh water loss from the basin is greater than that supplied by river inflow).

Observations from three Californian estuaries represent the essential spatio-temporal density structures during dry mediterranean climate summers. However, limited published data from estuaries in other mediterranean regions suggest that the structures observed in California are likely to be found in many of the estuaries of southwestern Australia, southwestern South Africa, Portugal, Morocco, Chile, northwestern Mexico, and so on.

In the following, a simplified estuarine basin is considered (Fig. 1). This basin receives freshwater via river inflow R and precipitation P while it loses freshwater through evaporation E'. Heat is exchanged with the atmosphere (heat flux Q). The temperature, salinity and density of this basin depends on the strength of these inputs/outputs and on the rate of hydrodynamic exchange with the adjacent ocean (the ambient). This hydrodynamic exchange is expressed as the sum of subtidal advection U and subtidal diffusion K. Following Largier, et al. (1995), the basin is considered to be a "hypersaline estuary" if its salinity is significantly greater than the ocean salinity (i.e., exceeds ocean salinity by at least one standard

deviation of ocean salinity fluctuations). A "thermal estuary" describes a basin in which the density structure is dominated by temperature. An "inverse estuary" is one in which the density of the water exceeds that in the ocean.

OBSERVATIONS

Hypersaline conditions, a clear indicator of low freshwater inflow, have been observed in many estuaries along the Pacific coast of the Californias (Fig. 2). In Tomales Bay, the northernmost of these basins, temperature and salinity data have been collected over a 7-year period (Largier, et al., 1995). The seasonal cycle is dramatic, dominating any inter-annual fluctuations (Fig. 3). Winters are cold and wet, yielding large river inflow and low salinities. Summers are warm and dry, resulting in net evaporation and high salinities. Occupying a rift valley along the San Andreas fault, this basin is long and thin. Temperature, salinity and density data are clearly functions of the distance from the ocean, at one end, and from the major river flowing in at the other end. At station 16, 16 km from the mouth and 4 km from the head, salinities drop into the mid-20's while temperatures drop below 10°C during winter. In summer, salinities exceed ocean values by about 2 and temperatures exceed ocean values by several degrees centigrade. While estuarine temperatures rise during early summer, ocean temperatures remain low as a result of wind-driven upwelling along the ocean coast (Lentz, 1991; Largier, et al., 1993). The summer gradient in temperature maintains a positive density gradient (a "thermal estuary"). It is only in the fall, when estuary temperatures drop, that the density gradient approaches zero and may become inverse owing to the hypersalinity of the basin, which persists until the onset of winter rains.

The coarse temporal resolution of Tomales Bay data does not allow one to ascertain whether a steady state salt balance occurs during late summer. In

Mission Bay, where data were collected more frequently, a quasi-steady salinity and temperature distribution is observable from June to September (Fig. 4). In this basin, hypersaline conditions are only observed in the one-dimensional side branches and not in the more complex morphology of the middle and outer bay. As in Tomales Bay, inverse conditions are only observed following the decrease in water temperatures in the fall and early winter, prior to rainfall. In Mission Bay, the hypersalinity is stronger and when the temperature gradient reverses in early winter a significant inverse structure is observed. This density head persists, however, indicating the absence of a singular density-driven flushing event in 1992. Rather, a steady salinity indicates that freshwater loss via evaporation is balanced by a seaward salt flux due to tidal diffusion mechanisms.

A similar seasonal cycle and longitudinal structure is observed in San Diego Bay. In this longer system (Fig. 5), one notices the separation between the region where increasing temperature dominates the density change ("thermal estuary") and the region where the increasing salinity dominates density change ("hypersaline estuary"). The middle and outer bay is thus characterized by a positive density gradient while the innermost part of the bay is characterized by a negative density gradient ("inverse estuary"). A density minimum is found inbetween these outer and inner regions. Reviewing Tomales Bay and Mission Bay data, a similar offset of temperature and salinity can be seen in the density structure (this is not clearly shown in this paper).

THE LONGITUDINAL SALT BALANCE

Noting the occurrence of hypersalinity in systems with long, narrow basins or in long, narrow branches of systems, Largier, et al. (1995) use a one-

dimensional model of vertically averaged salinity to illustrate the essence of the subtidal salt balance of these low-inflow estuaries.

$$\partial_t S = \partial_x \left[\left[\frac{R}{wh} + \frac{P x}{h} - \frac{E' x}{h} \right] S - K \partial_x S \right] \tag{1}$$

where h is the basin depth, w is the basin width, x is the longitudinal distance from the head of the estuary, t is time, K is the subtidal diffusion in the longitudinal direction and E', R and P are as earlier (Fig.1). Using $E = E'\text{-}P\text{-}R/wx$ as net evaporation, and expecting a quasi-steady salinity distribution in mid-summer ($\partial_t S = 0$), one can solve for $S(x)$. In all three systems studied, longitudinal dispersion appears to be a continuous subtidal process. Using a mixing length expression for the longitudinal diffusivity $K=kx^2$, one obtains the solution

$$\frac{S}{S_0} = \left[\frac{x}{L} \right]^{-E/kH} \tag{2}$$

which fits well to observed data from San Diego Bay (Fig. 6). From the longitudinal salinity distribution one can estimate the average residence time of water at a particular distance from the ocean (assuming constant salinity S_o), using the bulk expression

$$\tau_{res} = \frac{(S - S_0)h}{E\,S} \tag{3}$$

Average residence times increase markedly towards the head of the basin with negligible inflow. This is consistent with the marked decrease in the value of the tidal diffusivity, $K=kx^2$, obtained from a mixing length model. This long residence, relative to the time scales of surface fluxes (e.g., evaporation), is the defining dynamical character of these hypersaline basins.

Largier, et al. (1995) find that this simple one-dimensional approach adequately represents the salinity distributions of 5 illustrative examples: San

Diego Bay, Mission Bay and Tomales Bay, which are discussed in this paper, and Elkhorn Slough (California) and Langebaan (South Africa). Residence times in the hypersaline inner basin vary from 10 to 100 days.

SURFACE BUOYANCY FLUXES

While salinity is a useful conservative tracer of water residence, to understand density structures and potential buoyancy-driven exchange, one has to consider the simultaneous changes in salinity and temperature. This is particularly true for mid-latitude west coast regions which are characterized by coastal upwelling, cool ocean waters and significant temperature gradients. In tropical systems, where the ocean is warm, temperature gradients are less important (Wolanski, 1986). In freshwater "estuaries" connected to large lakes, temperature is all important as there is no active salinity effect (Hamblin and Lawrence, 1990).

As noted, the outer and middle San Diego Bay exhibits a significant temperature gradient whereas the maximum salinity gradient occurs farther into the bay. The resultant density minimum is clearly illustrated on a temperature-salinity plot (Fig. 7). This key structure of low-inflow west coast estuaries can be illustrated with a very simple model of heating and evaporation. Bulk formulae for surface heating (e.g., Gill, 1982) can be reduced, through approximation, to a simple dependence on the time that a water parcel has been within the estuary:

$$\begin{aligned} Q &= Q_{other} + \rho_a c_p D_h u (T_a - T_s) \\ &= q(T_{eff} + T_a - T_s) \end{aligned}$$

Q_{other} represents the heat flux terms other than sensible heat flux. These other heat flux terms are expected to have a much weaker dependence on the increasing

surface water temperature, and are treated as constant in this simplification. They are represented by an effective constant temperature addition T_{eff} to atmospheric temperature T_a. The coefficient q is a product of air density ρ_a, heat capacity of the air c_p, wind speed u, and a dimensionless heat transfer coefficient (Stanton number) D_h. The change in temperature is then

$$\partial_t T = \frac{Q}{c_w \rho h} = b - c\,T_s$$

where

$$b = (Q_{other} + \rho_a c_p D_h u\, T_a)/c_w \rho h$$

and

$$c = \rho_a c_p D_h u / c_w \rho h$$

ρ is the water density, c_w the heat capacity of the water and h the water depth. Thus, the temperature of a parcel of water that has been resident in the basin for time t is given as

$$T(t) = \frac{b}{c} - d\,e^{-ct} \tag{4}$$

where $d = \frac{b}{c} - T(t{=}0)$

This expresses the time-dependent increase in shallow water temperature as simply dependent on the time-dependent surface temperature (assuming constant wind, air temperature, humidity, insolation and vapour pressure). The water heat content is saturated (under these constant conditions) when T_s increases to balance T_a+T_{eff}.

Under these conditions, evaporation occurs at an approximately constant rate, being only weakly dependent on surface temperature and salinity. Thus,

$$S(t) = \frac{S_o}{1 - E\,t/h} \tag{5}$$

Starting with ocean water of temperature12°C and salinity 33 at time t=0 (as it enters the shallow-water basin), and assuming conditions representative of a low-inflow California estuary, the asymptotic increase in temperature and the constant increase in salinity are plotted for a 100-day period (Fig. 8). Initially, density decreases due to warming (net positive buoyancy flux). Later, once the heat content of the water is saturated, the continuing increase in salinity leads to an increase in density (net negative buoyancy flux). A density minimum is noted after a time period of about a month. If the San Diego Bay data from August 1993 are plotted against estimated residence time, given by Eqn. (3), the same structure is observed (Fig. 9).

LONGITUDINAL DENSITY STRUCTURE

The time history of water in a quasi-steady system is reflected in the distance of water parcels from the ocean. Water further from the ocean is older on average, as described by the one-dimensional diffusion model of these long, narrow basins. Using the solution for $S(x)$ under the assumption of $K = kx^2$, as in Eqn. (2), and estimating residence time by the degree of hypersalinity, one obtains a simplified longitudinal variation in residence time:

$$\tau_{res}(x) = \frac{h}{E}\left[1-(\frac{x}{L})^{E/kh}\right]$$

which can be written as

$$x(\tau_{res}) = L\left[1-\frac{E\,\tau_{res}}{h}\right]^{kh/E} \qquad (6)$$

where x is the distance from the head at which a given residence time τ_{res} would occur in this simplest one-dimensional model (Fig. 10a). Using this time-to-space conversion, one obtains the expected spatial increase in temperature and salinity due to the temporally integrated model heat input and freshwater removal (Fig. 10b,c). Further, from these $T(x)$ and $S(x)$ distributions, one obtains the longitudinal density distribution $\rho(x)$ (Fig. 10d) and the longitudinal gradient in density (Fig. 10e).

Wherever the longitudinal density gradient is strong enough, one may expect it to drive a stratified exchange flow - cold, dense seawater intruding as a basal flow near the mouth and salty, dense inner basin water draining seaward as a basal flow near the head. Following Linden and Simpson (1988), the buoyancy-driven diffusivity is proportional to $|\partial_x \rho|.h^2$. With typical model output (Fig. 10), then, one can expect maximum buoyancy effects in the deeper thermal outer estuary and in the high-gradient hypersaline region towards the head of the estuary (Fig. 10h, Fig. 11). In contrast, simple tidal diffusivity, which is proportional to x^2, decreases strongly towards the head of the basin where $x \rightarrow 0$ (Fig. 11). Thus, it is in the hypersaline region near the head of the estuary that density-driven exchange is likely to be a significant component of the longitudinal diffusion. Transient hypersaline-related inverse circulation has been observed at the landward ends of both San Diego and Mission Bays. Although weak, the observed structures are clearly due to the relaxation of the inverse density distribution. In Fig. 12, the density minimum as well as the two regions of stratified exchange flow are evident. These coherent vertical structures are transient, disappearing tidally. The detailed hydrodynamic structures of the "thermal estuary" part of San Diego Bay are discussed by Chadwick, et al. (1995). Aspects of the role of buoyancy exchange in Tomales Bay are addressed through a model study of historical depth changes in Tomales Bay (Hearn, et al., 1995).

The strongest evaporation-associated inverse circulation is expected in deep systems, with relatively weaker vertical mixing, e.g., the Mediterranean Sea (Lacombe and Richez, 1982) and Spencer Gulf (Nunes Vaz, et al, 1990). However, significant inverse circulation, albeit transient, can be expected in evaporative estuaries with extensive shallows, to enhance the net evaporative loss of freshwater, and deep channels, in which density exchange flow can occur. An example is Laguna Ojo de Liebre (Postma, 1965, eg., Fig 12a). It appears that significant inverse circulation is also found in tidal creeks through mangrove swamps, due to the large evapotranspiration through the mangrove plants (e.g., Maputo Bay, Mocambique, A. Hoguane, pers. comm.).

CONCLUSION

In many mediterranean climate, west coast estuaries one can identify up to 4 distinct hydrodynamic regimes. The presence and extent of these regimes varies seasonally. Closest to the mouth, a "marine" regime is typically found. Residence times are comparable to the tidal period, temperature and salinity are similar to oceanic values and diffusivity is dominated by tidal effects, particularly tidal pumping. With increased distance from the sea (at least one tidal excursion), residence times increase to several days and significant temperature gradients are observed. This "thermal" regime is distinguished by large Q/h and it is absent in regions where the oceanic source water is warm. At longer residence times, found deeper into the basin, the heat content is saturated and an evaporative increase in salinity dominates the surface buoyancy flux (E/h is large). This is the "hypersaline" regime where inverse circulation may be observed. In some systems, a small freshwater inflow $R << EwL$ (where L is the basin length) persists during the dry season and an "estuarine" regime may be observed at $x<R/Ew$.

s some evidence that density-driven circulation occurs in the thermal regime
Sa Diego Bay (this paper, and Chadwick, et al., 1995), Hamilton Harbor
lin and Lawrence, 1990) and Hilary Harbor (Schwartz and Imberger, 1988) -
hypersaline regime - e.g., San Diego and Mission Bays (this paper) and
a Ojo de Liebre (Postma, 1965) - and in the estuarine regime - e.g., Van
ns Gulf (Wolanski, 1986). But, it is not clear how important this transient
ed exchange is to the net longitudinal exchange in tidal basins. It is clear,
er, that regions of near-zero gradient $\partial_x \rho$ exist and that these regions must be
ated by tidal action. Any closed circulation cells, as suggested by Wolanski
), are likely to occur in non-tidal estuaries only.

The seasonal temperature cycle tends to lead the seasonal salinity cycle by a
or two, as in Tomales Bay, because of low estuarine salinities and cold
led oceanic water in spring. This is due to residual river inflow in spring, the
rapid response of the basin to heating/cooling and the delay in winter rains
ve the day length (and heat cycle). Owing to this temporal lag, much of a
ornian estuary is characterized by a "thermal" regime in early summer and by
persaline" regime in the fall. In the presence of tidal stirring, double diffusive
ty-temperature gradients and the potential for nocturnal overturn, the degree
rtical mixing is unclear. It is the interaction of these complex vertical mixing
sses with the longitudinal density head that will determine the importance of
ce buoyancy fluxes in enhancing estuary-ocean exchange in low-inflow
ms.

Schwartz, R. A., and Imberger, J. 1988. Flushing behaviour of a coastal marina. *Environmental Dynamics Ref.*, ED-88-259, University Western Australia, Nedlands, Australia.

Lacombe, H. and Richez, C. 1982. *The regime of the Straits of Gibraltar. In: Hydrodynamics of Semi-enclosed Seas*, (J.C.J. Nihoul, ed.), Elsevier, Amsterdam, 13-73.

Largier, J. L., Magnell, B. A. and Winant, C. D. 1993. Subtidal circulation over the northern California shelf. *J. Geophys. Res.*, *98*(C10), 18,147-18,179.

Largier, J. L., Hollibaugh, J. T., and Smith, S. V. 1995. Seasonally hypersaline estuaries in mediterranean climate regions. *Est: Coast. and Shelf Sci.* (submitted).

Lentz, S. J. (ed.), 1991. *CODE (Coastal Ocean Dynamics Experiment)*, A collection of reprints. 817 pp., Woods Hole Oceanographic Institution, Woods Hole, MA.

Linden, P. F., and Simpson, J. E. 1988. Modulated mixing and frontogenesis in shallow seas and estuaries. *Cont. Shelf Res, 8*, 1107-1127.

Nunes Vaz, R. A., Lennon, G. W. & Bowers, D. G. 1990 Physical behaviour of a large, negative or inverse estuary. *Cont. Shelf Res.,10*(3), 277-304.

Postma, H. 1965. Water circulation and suspended matter in Baja California lagoons. *Neth. J. Sea Res.*, *2*(4), 566-604.

Pritchard, D. W. 1967. Observations of circulation in coastal plain estuaries. In: *Estuaries* (G.H.Lauff, ed.), AAAS Publ. #83, Washington, 37-44.

Wolanski, E. 1986 An evaporation-driven salinity maximum zone in Australian tropical estuaries. *Est. Coast. Shelf Sci.*, *22*, 415-424.

Figure 1. Schematic and definition of significant water and heat exchanges in a low-inflow estuary (variables defined in text).

Figure 2. Seasonally hypersaline estuaries along the west coast of North America. (a) Location of various systems in which hypersalinity has been reported. (b) Position of CTD stations in Tomales Bay and typical region of hypersalinity in late summer (shaded). (c) Mission Bay stations and hypersaline region. (d) San Diego Bay stations and hypersaline regions.

Figure 3. Multi-year seasonal variation of vertically averaged temperature, salinity, and density in Tomales Bay, as a function of distance from the head ($x = 0$). Regions of water that are warmer and saltier than the ocean are hatched (summer). Regions of freshwater influence are seen in winter.

Figure 4. The seasonal variation in temperature, salinity, and density in Mission Bay. At station 21 (farthest from ocean, Figure 2c), surface values (open circles), bottom values (crosses), and vertical average values (bold line) are plotted. For comparison, vertical average values are also plotted for station 9, at the landward extent of the well-flushed outer estuary (dashed line), and for Scripps pier, several kilometers north of the mouth (solid line). The period during which station 21 is warmer, saltier or denser than the ocean is indicated by shading. Stratifiction is not observed in the hypersaline inner estuary. The date marks indicate the start and end of hypersaline and inverse conditions.

Figure 5. Vertically averaged temperature, salinity, and density for San Diego Bay on 3 days in August 1993 (symbols). Solid line is average of three data sets which exhibit tidal differences. Data are plotted as distance from the mouth.

Figure 6. In the top panel, the solution from Eqn. (2), plotted as line, is fitted to observed vertically averaged salinity (from line in Fig. 5), plotted as asterisks. The middle panel presents diffusivity $K = kx^2$ as a function of distance from the head x, with the value of k obtained from the fit in the top panel. Asterisks are obtained from balancing advection and diffusion at each station (assuming steady salinities, see Largier, et al., 1995). In the bottom panel, residence time is plotted - values are calculated from Eqn. (3).

Figure 7. Vertically averaged temperature-salinity data from San Diego Bay (August 1993, see Fig. 5) plotted over a density field.

Figure 8. Model results for the increase of temperature from Eqn. (4) and the increase of salinity from Eqn. (5) as a function of time that a water parcel has been resident in a shallow, zero-inflow basin. Parameter values are those typical of Californian systems. The temporal decrease and subsequent increase in calculated density is shown in the bottom panel.

Figure 9. Observed temperature, salinity, and density values in San Diego Bay (August 1993, Fig. 5) plotted as a function of residence time, estimated from Eqn. (3).

Figure 10. (a) Model residence times obtained from Eqn. (6), with parameter values being typical of those in California. (b) Model temperature, given residence time from first panel and heating modeled by Eqn. (4). (c) Model salinity, given residence time from first panel and salinity increase over time modeled by Eqn. (5). The solid line indicates how salinity values increase if the basin shoals markedly towards the head (e.g., sixth panel). (d) Density calculated from model temperature and salinity. Solid line is for adjusted salinity (as in third panel). (e) Longitudinal density gradient. (f) Illustrative longitudinal depth profile, allowing for enhanced hypersalinity in the shallow regions at the head of the estuary. (g) The square of depth as a function of longitudinal position. (h) The typical longitudinal dependence of buoyancy diffusivity values in a low-inflow estuary, based on the dependence given by Linden and Simpson (1988). Diffusivity units are arbitrary.

Figure 11. The typical buoyancy diffusivity profile $K \alpha |\partial x \rho| h^2$ for a low-inflow estuary (see Fig. 10) compared with a typical tidal diffusivity profile $K \alpha x^2$. Both diffusivities are normalized; tidal values are represented by a dashed line. An additional solid line represents the shape of buoyancy diffusivities that are an order of magnitude smaller than the tidal values. In this case, buoyancy diffusivities exceed tidal diffusivities in the strongly hypersaline region close to the head (over the shallow region within 5-10 km from the head of this model basin).

Figure 12. Schematic of the longitudinal temperature, salinity, and density profiles that may result in up to four distinct regimes in a Californian LIE. The marine outer basin is dominated by tidal diffusion. The thermal regime is characterized by a positive density gradient. The hypersaline regime is characterized by a negative density gradient, and the riverine regime is characterized by a positive density gradient due to river inflow. A density minimum may be observed in mid-estuary and a density maximum at or near the head of the basin (e.g., Fig. 7).

FIG 1

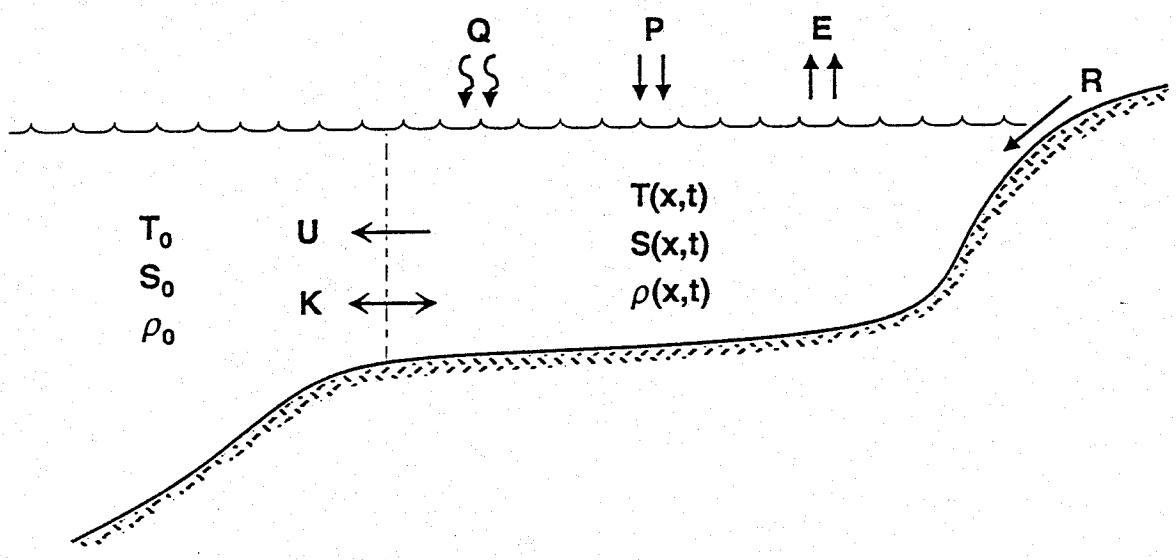

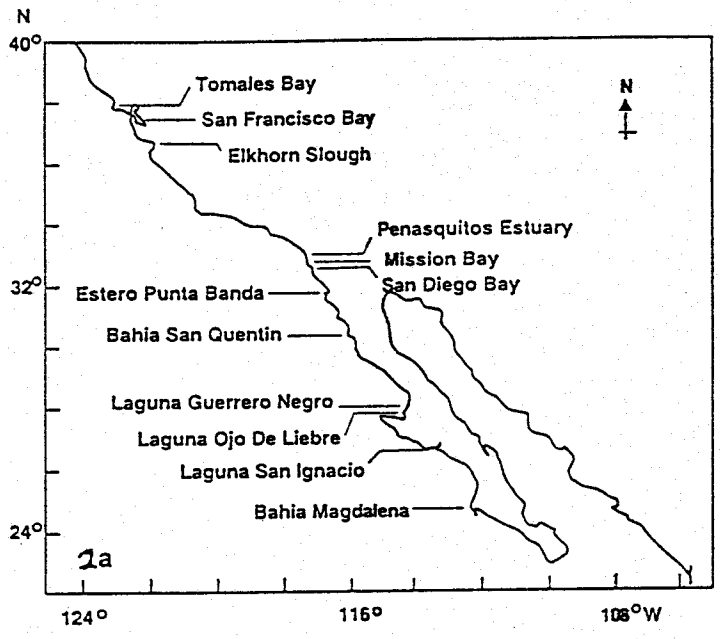
N
40°
32°
24°
Tomales Bay
San Francisco Bay
Elkhorn Slough
Penasquitos Estuary
Mission Bay
San Diego Bay
Estero Punta Banda
Bahia San Quentin
Laguna Guerrero Negro
Laguna Ojo De Liebre
Laguna San Ignacio
Bahia Magdalena
1a
124°
116°
108°W

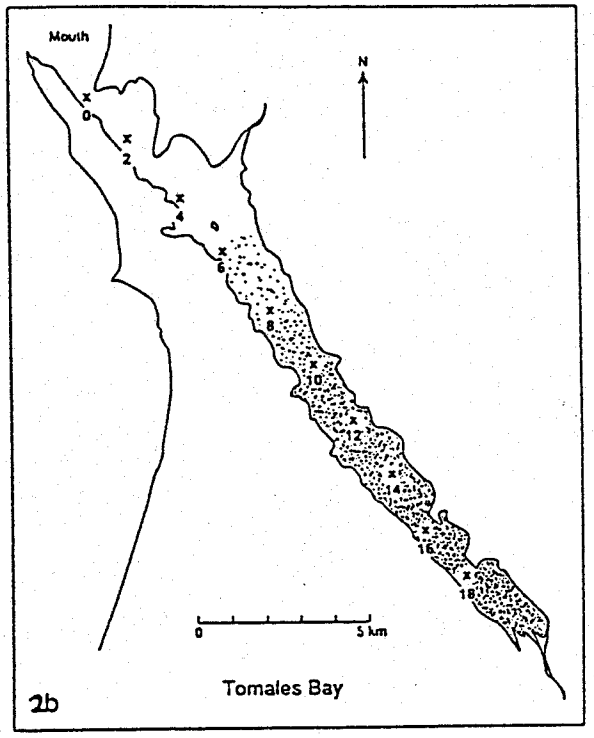
Mouth
N
0
2
4
6
8
10
12
14
16
18
0
5 km
2b
Tomales Bay

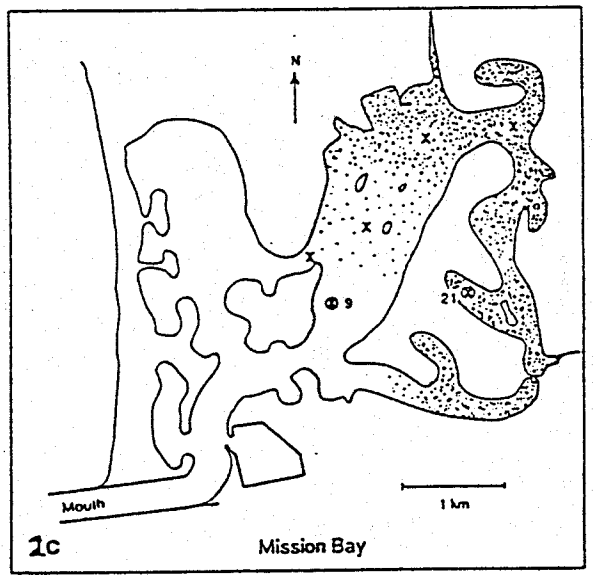
N
Mouth
1 km
1c
Mission Bay

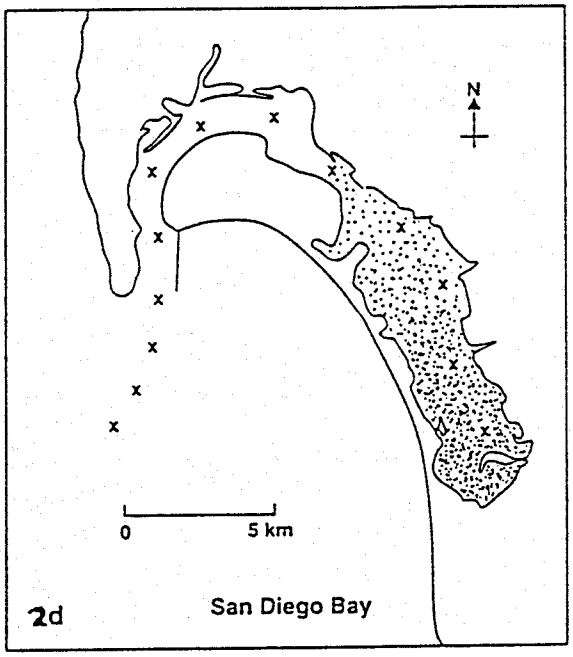
N
0
5 km
2d
San Diego Bay

FIG. 2

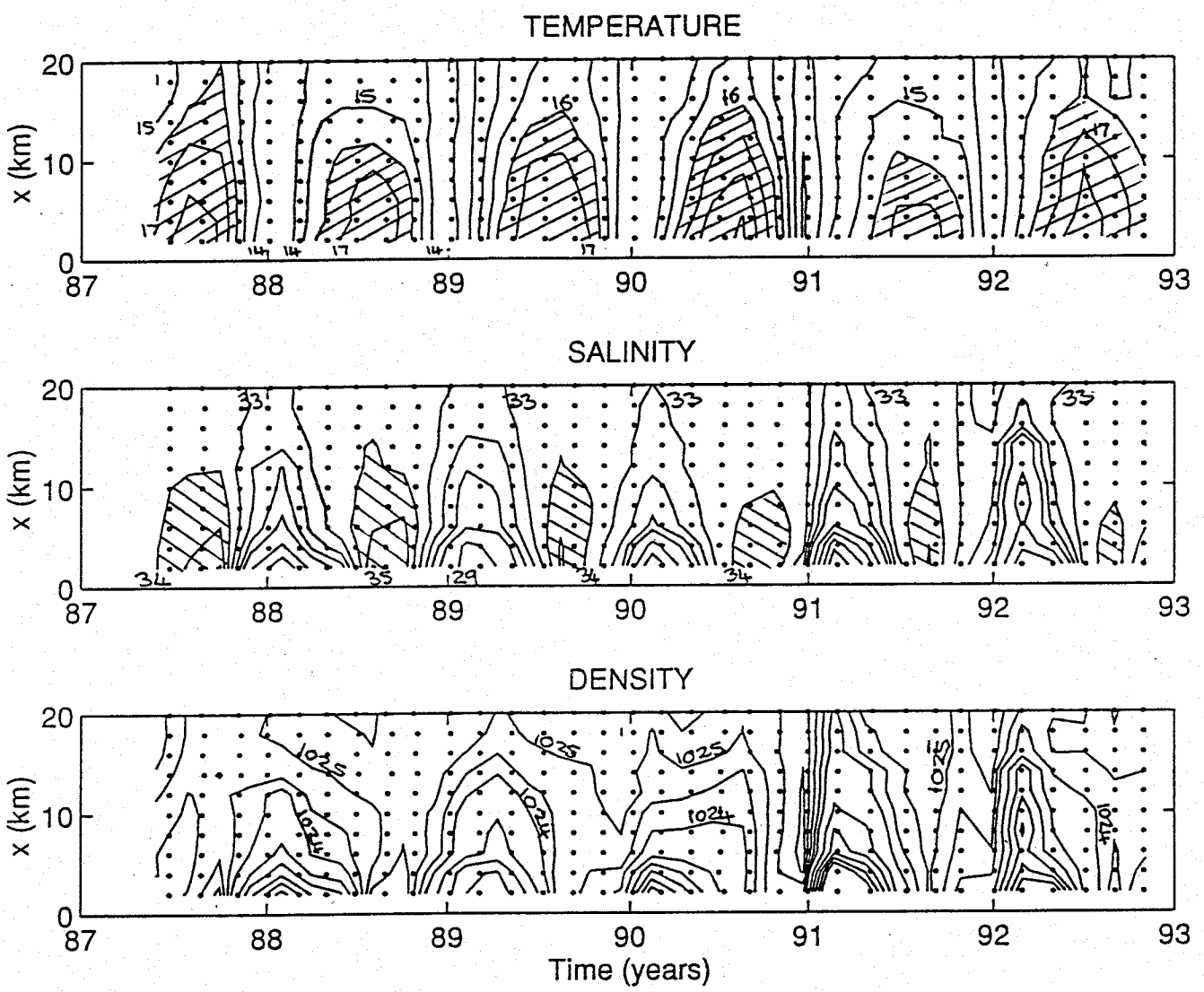
TEMPERATURE
SALINITY
DENSITY
x (km)
20
10
0
87
88
89
90
91
92
93
Time (years)

Fig. 3

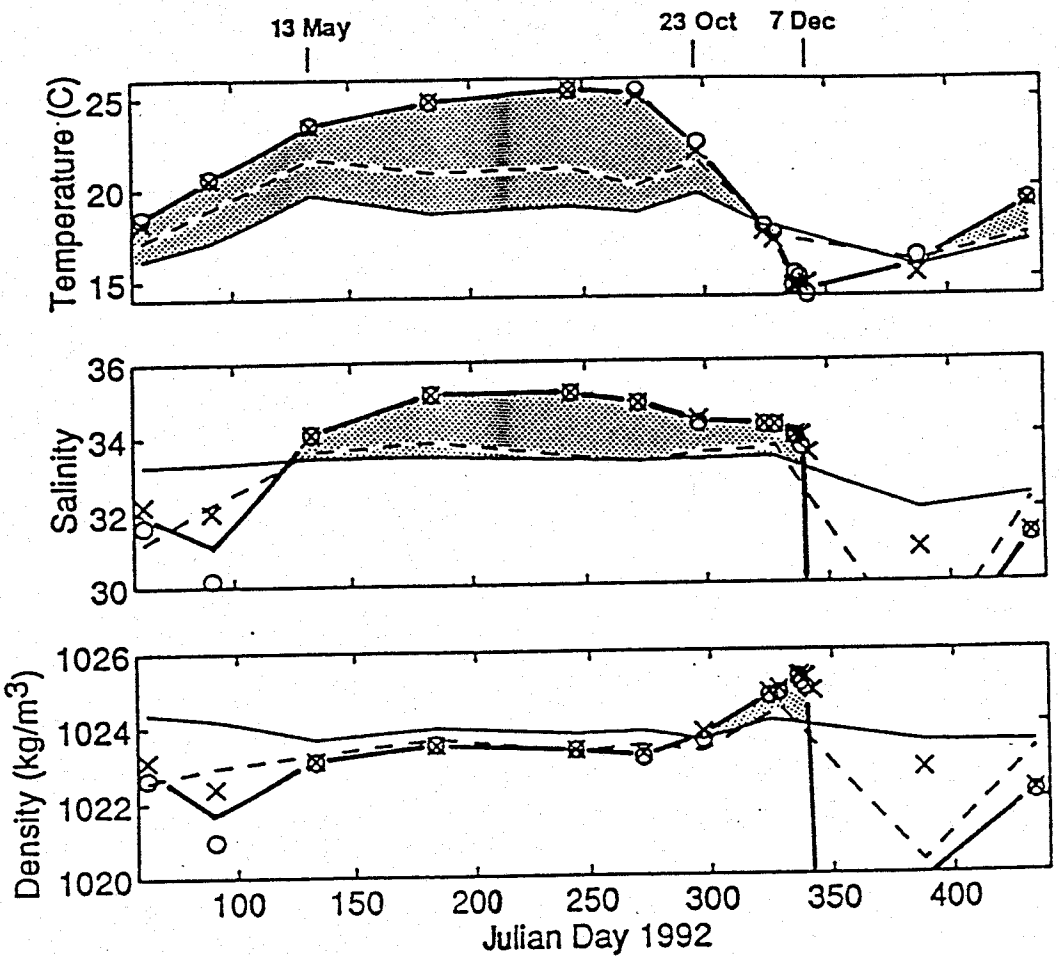
13 May
23 Oct
7 Dec
Temperature (C)
25
20
15
Salinity
36
34
32
30
Density (kg/m3)
1026
1024
1022
1020
100
150
200
250
300
350
400
Julian Day 1992

FIG. 4

Fig. 5

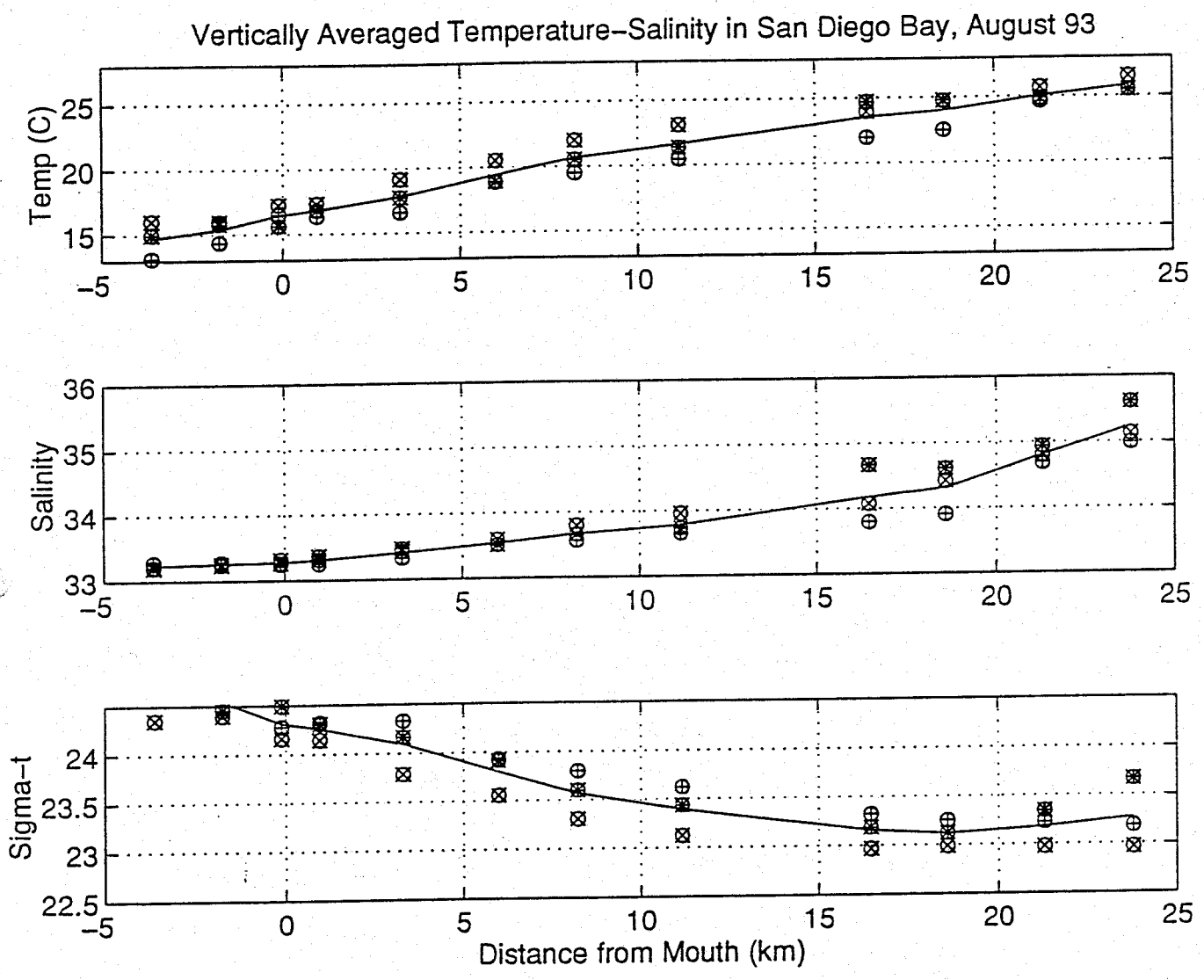
Vertically Averaged Temperature–Salinity in San Diego Bay, August 93
Temp (C)
25
20
15
−5
0
5
10
15
20
25
Salinity
36
35
34
33
Sigma–t
24
23.5
23
22.5
Distance from Mouth (km)

Fig. 5

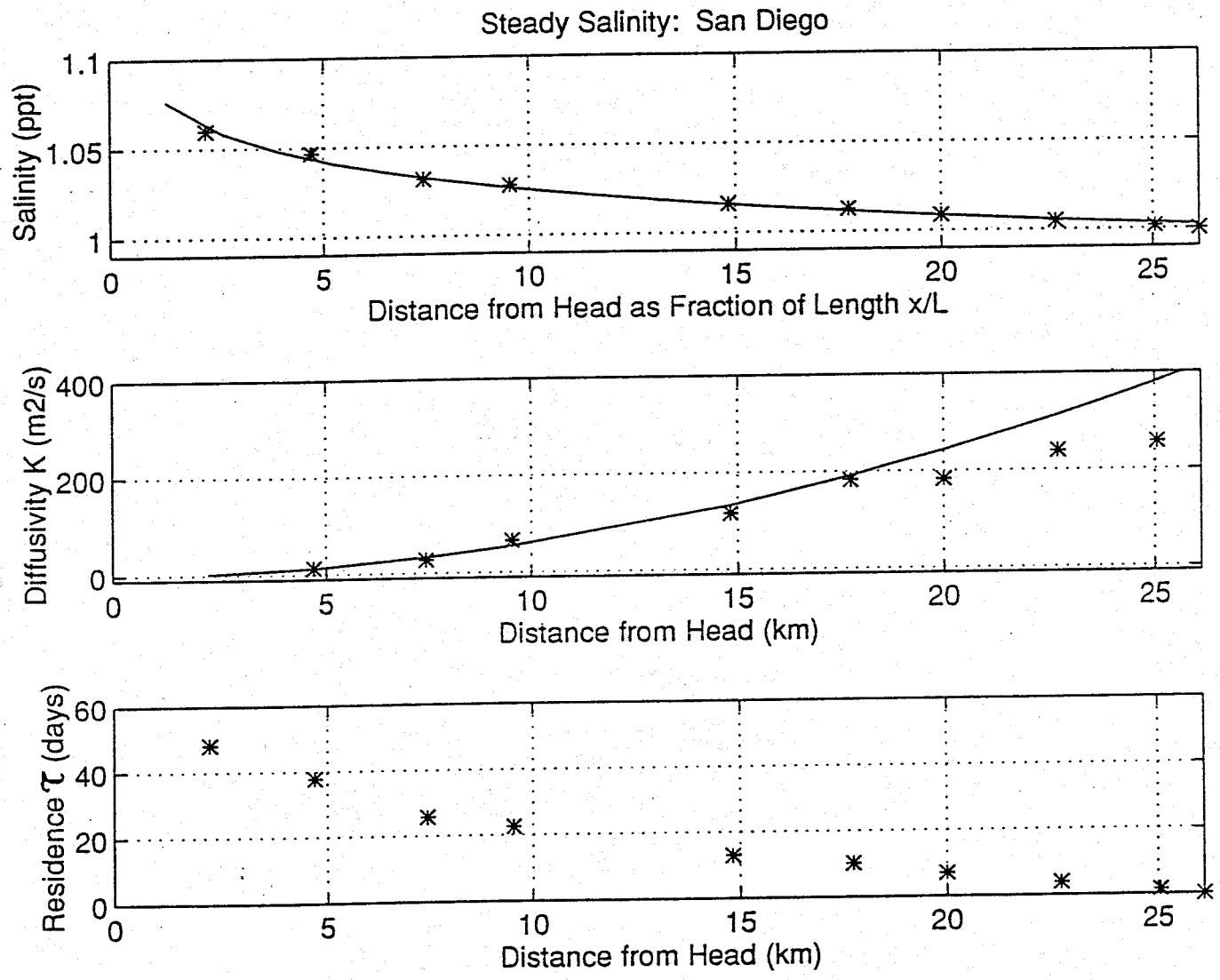
Steady Salinity: San Diego
Salinity (ppt)
1.1
1.05
1
0
5
10
15
20
25
Distance from Head as Fraction of Length x/L
Diffusivity K (m2/s)
400
200
0
Distance from Head (km)
Residence τ (days)
60
40
20
Distance from Head (km)

Fig. 6

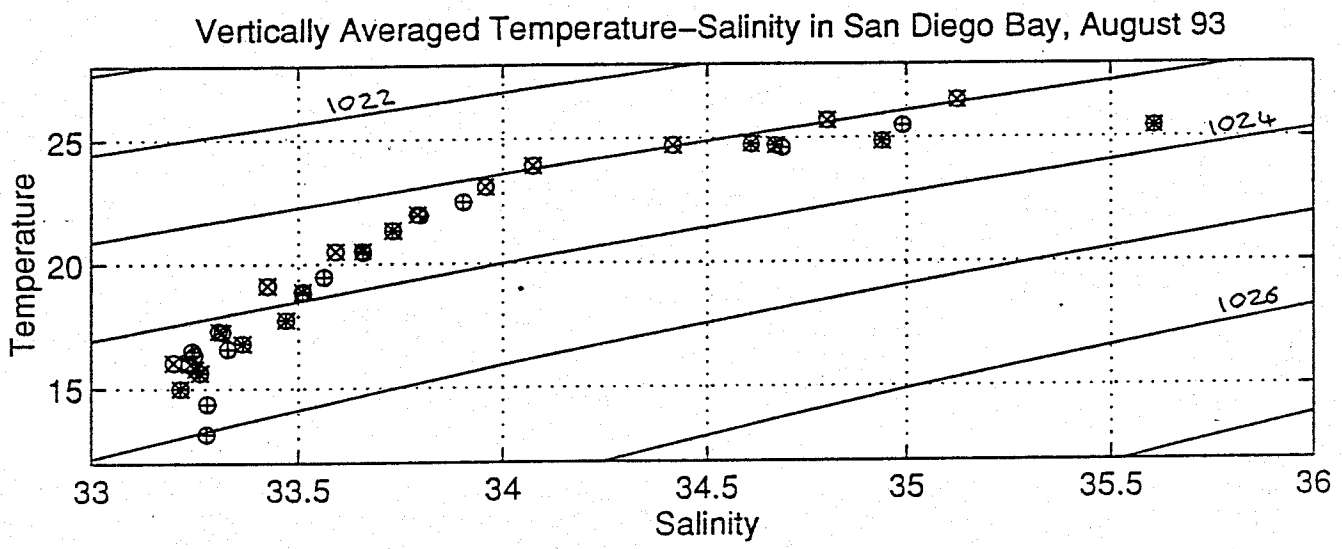
Vertically Averaged Temperature–Salinity in San Diego Bay, August 93
1022
1024
1026
25
20
15
Temperature
33
33.5
34
34.5
35
35.5
36
Salinity

Fig. 7

Fig. 8

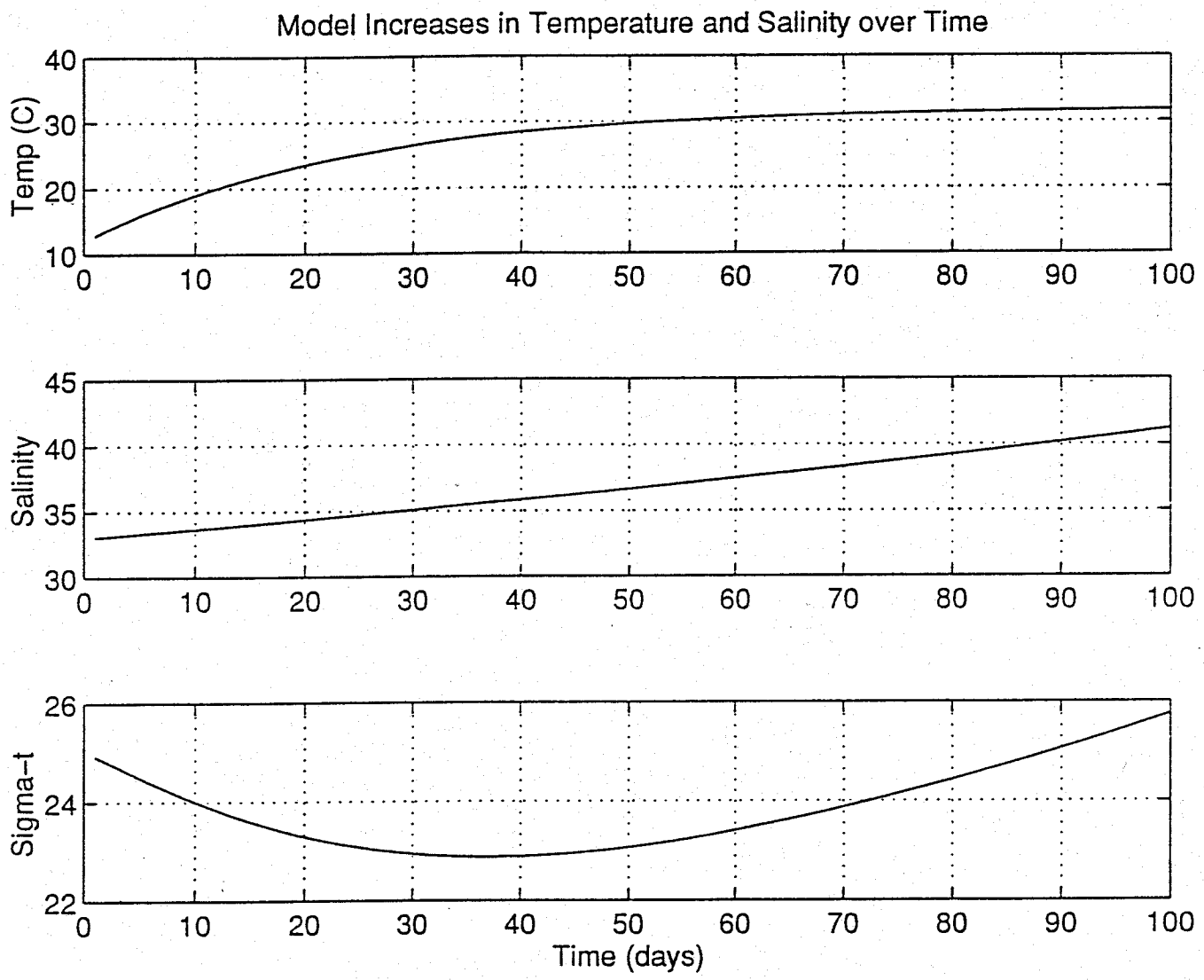
Model Increases in Temperature and Salinity over Time
Temp (C)
40
30
20
10
0
10
20
30
40
50
60
70
80
90
100
Salinity
45
40
35
30
Sigma-t
26
24
22
Time (days)

Fig. 9

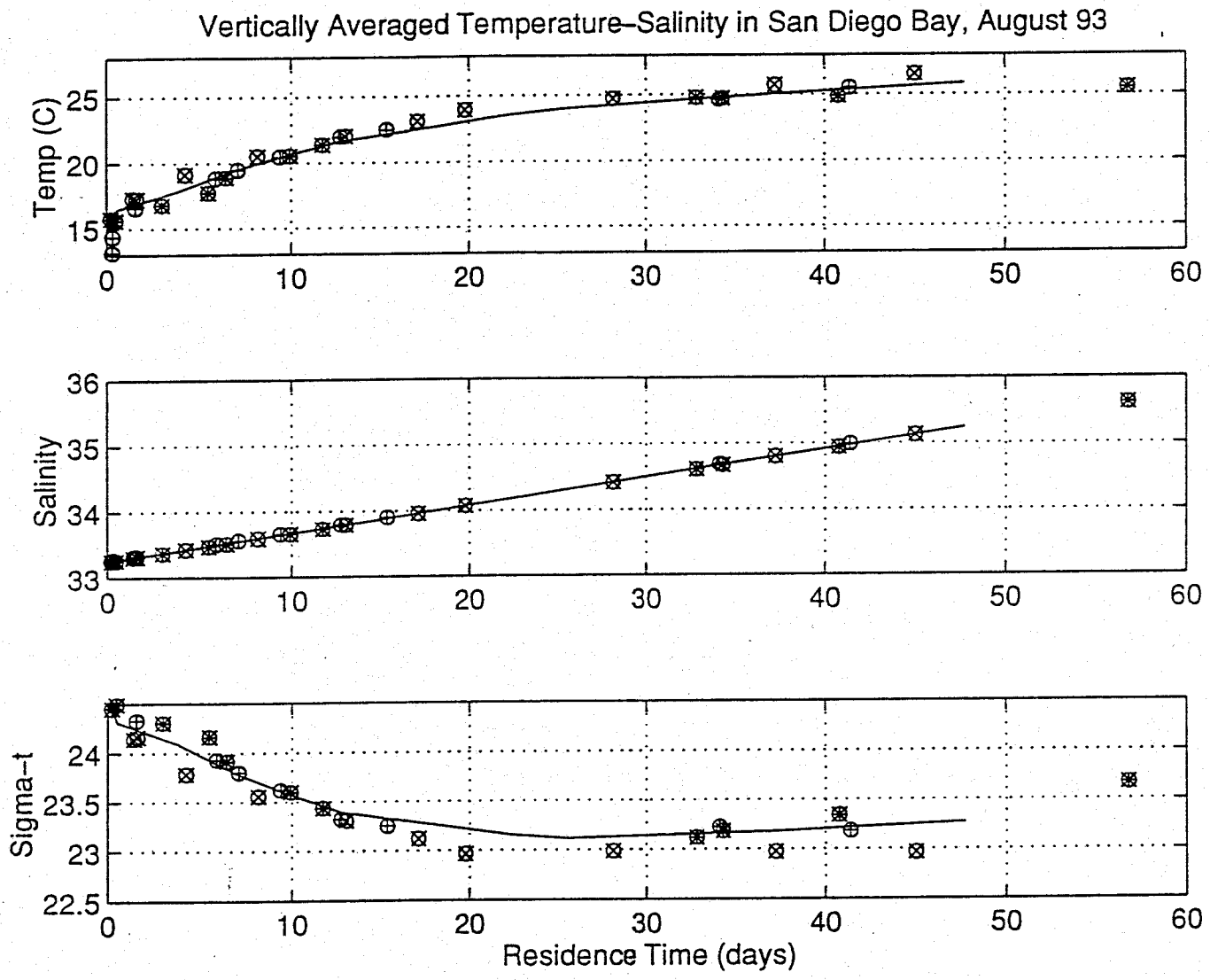
Vertically Averaged Temperature–Salinity in San Diego Bay, August 93
Temp (C)
25
20
15
0
10
20
30
40
50
60
Salinity
36
35
34
33
Sigma–t
24
23.5
23
22.5
Residence Time (days)

Fig. 10

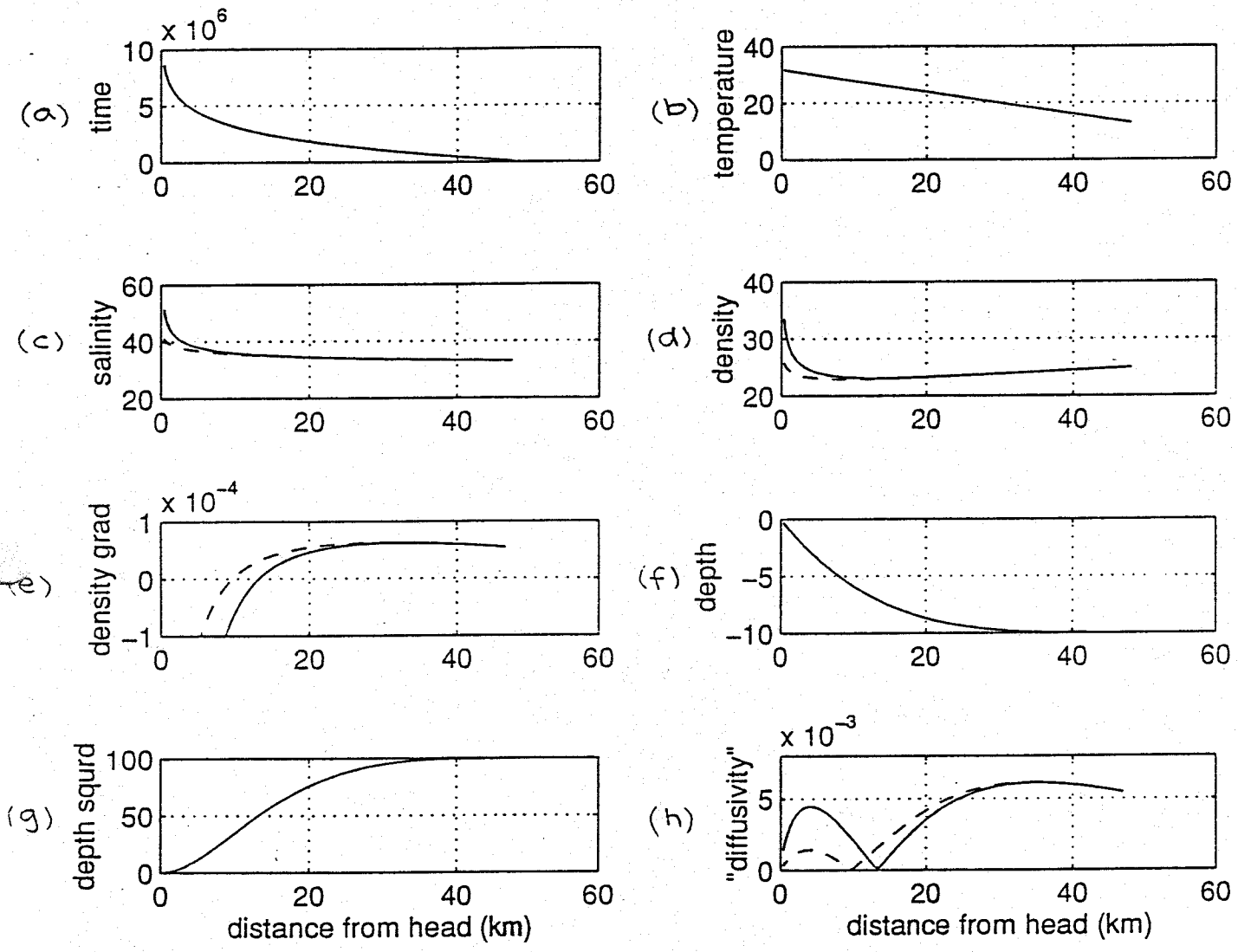
(a)
time
x 10^6
10
5
0
0
20
40
60
(b)
temperature
40
20
0
0
20
40
60
(c)
salinity
60
40
20
0
20
40
60
(d)
density
40
30
20
0
20
40
60
(e)
density grad
x 10^-4
1
0
−1
0
20
40
60
(f)
depth
0
−5
−10
0
20
40
60
(g)
depth squrd
100
50
0
0
20
40
60
distance from head (km)
(h)
"diffusivity"
x 10^-3
5
0
0
20
40
60
distance from head (km)

Fig. 11

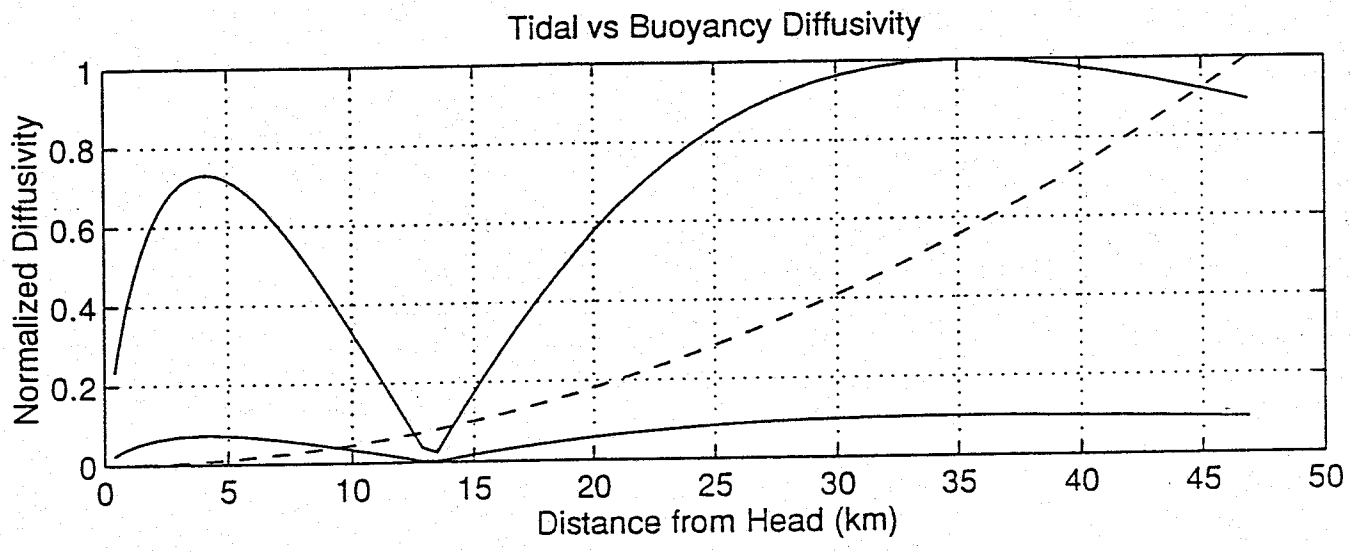
Tidal vs Buoyancy Diffusivity
Normalized Diffusivity
0
0.2
0.4
0.6
0.8
1
0
5
10
15
20
25
30
35
40
45
50
Distance from Head (km)

Fig. 12

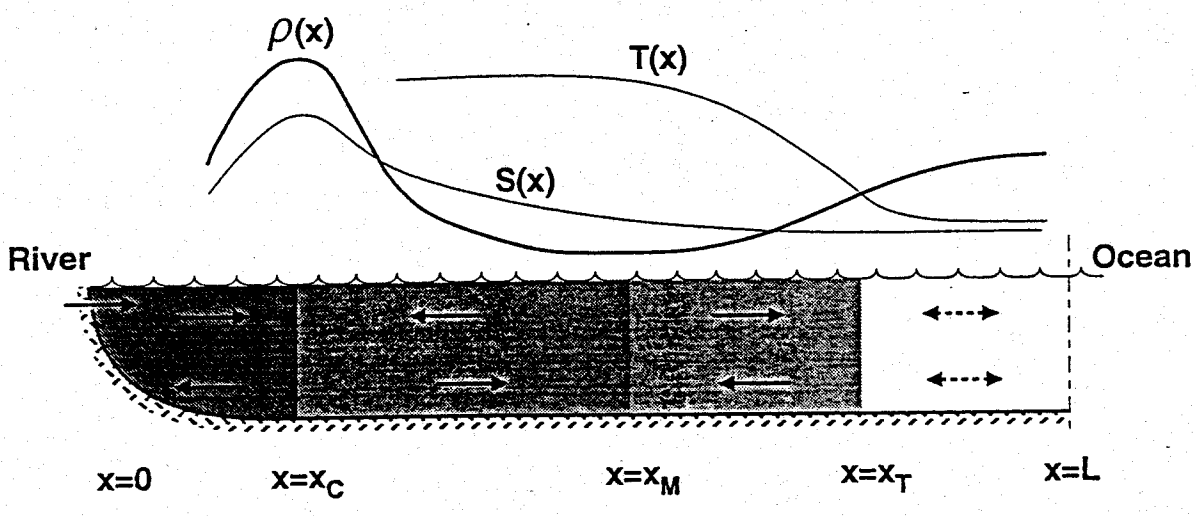

RIVERINE	HYPERSALINE	THERMAL	MARINE
$\partial_x S>0$	$\partial_x S<0$	$\partial_x T<0$	
$\partial_x \rho>0$	$\partial_x \rho<0$	$\partial_x \rho>0$	$\partial_x \rho \sim 0$